INTERNATIONAL JOURNAL OF
COASTAL, OFFSHORE & ENVIRONMENTAL ENGINEERING

Available online at: www. ijcoe.org

Hybrid Intelligence for Coastal Pattern Recognition: ANFIS-Based Prediction of Multi-Level Beach Cusp Spacing

Azadeh Valipour[1*]
Hossein Shirgahi[2]

[1*] *Department of Marine Science and Technology, Jo.C., Islamic Azad University, Jouybar, Iran; azadeh.valipour@iau.ac.ir*
[2] *Department of Computer Engineering, Jo.C., Islamic Azad University, Jouybar, Iran*

ARTICLE INFO

Article History:
Received: 16 April 2025
Accepted: 03 May 2025

Keywords:
Adaptive Neuro-Fuzzy Inference System
Machine learning
Coastal management
Membership functions
Neural network

ABSTRACT

Given the necessity of understanding coastal dynamics and predicting erosion in coastal areas, this research employs the Adaptive Neuro-Fuzzy Inference System as a machine learning model for predicting beach cusp spacing and subsequently optimizing coastal management. ANFIS has the advantage over other techniques to model the more complex nonlinear relationships involved in beach cusp formation. It learns from existing data, adapts to new information varying with coastal hydrodynamic conditions, and gives back to the user interpretability by showing underlying rules dictating cusp dynamics. This paper discusses implementing ANFIS to predict beach cusp spacing and examines its performance against a neural network. In this way, different ANFIS configurations were tested, and the effect of membership functions on the performance of the fuzzy system was investigated. The main outcomes of this research indicate that even though optimized Artificial Neural Network (ANN) models perform reasonably well for the upper beach face, the optimized ANFIS (trimf) model performs better in accuracy and stability for the middle and lower beach faces. This study effectively highlights the importance of selecting the optimal model tailored to each beach section's specific conditions and characteristics.

1. Introduction

Beach cusps are rhythmic features that form on the beach face after complex interactions between wind, waves, and currents with beach sediments. It is found that these shore-parallel features are more abundant at medium-energy, reflective beaches which have steeper beaches with coarser sediments [1].

Single- level beach cusps form as only one level of cusps on the beach face (Figure 1a); on the other hand, beach cusp systems can also occur at different levels on the beach face. When there are different levels of cusps lining a beach, this system would be called multi-level beach cusps (Figure 1b).

The levels may be lower, middle, and upper parts of the beach [2]. Lower beach cusps are more dynamic because these shift from one point to another as a result of a tidal cycle, while middle and upper beach cusps are fairly static and can be retained between tidal cycles [3]. Thus, beach cusps be classified into various groups according to their formation conditions and position on the beach profile [2]. Types of these features include Swash cusps, Storm cusps, and Low tide cusps, and each type has its peculiar features and formation processes (Figure 1c).

To investigate the morphodynamic behavior of these coastal features, familiarity with the definitions of relevant beach cusp parameters is essential. The most significant parameter for this type of coastal formation is the cusp spacing (C_s), defined as the horizontal distance along the shoreline between the apexes of two adjacent beach cusp horns.

Cusp elevation (C_e) is the vertical distance from the highest point on the beach cusp horn to the Mean Sea Level (MSL). Cusp depth (C_d) represents the vertical distance from the highest point on the beach cusp horn to the wave swash limit in the cusp bay. Lastly, cusp amplitude (C_a) is defined as the maximum vertical difference between the beach cusp horn and the cusp bay (Figure 1d).

To date, numerous theories have been proposed by various researchers to explain the formation and evolution of beach cusps (Table 1).

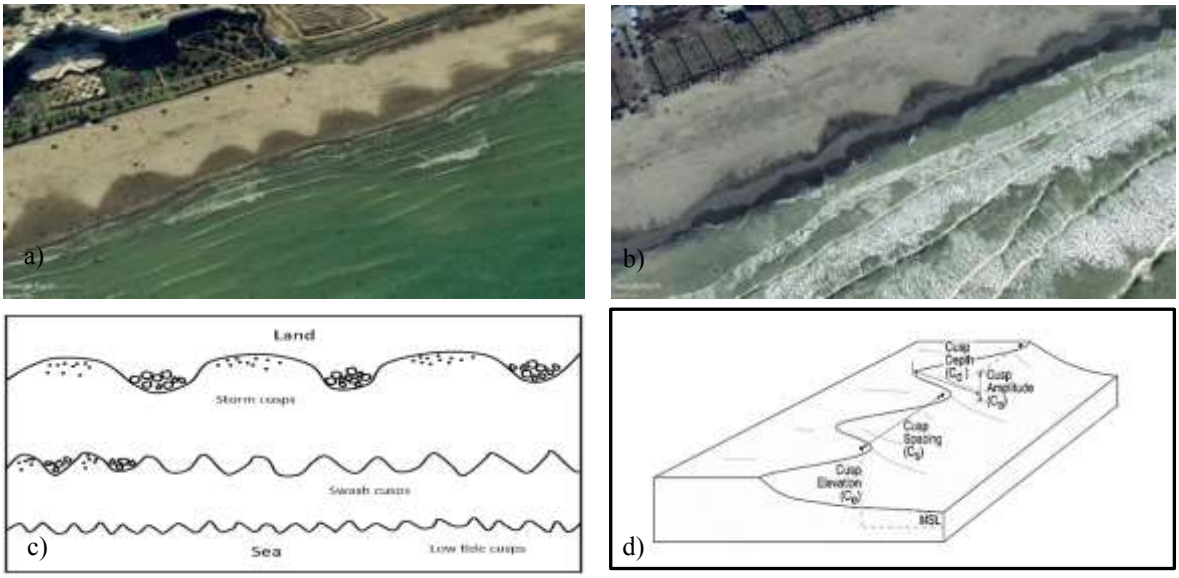

Figure 1. Google Earth view of the a) single-level beach cusps b) multi-level beach cusps c) Different types of beach cusps d) Schematic design of the definition of beach cusp parameters [4].

Some of these studies make it possible to estimate the spacing of beach cusps based on the hydrodynamic and morphodynamic conditions of the coast [5][6][7][8] [9]. However, the variable hydrodynamic conditions of the coast and the difficulties in determining sediment grain size due to the increasing use of mixed sand and gravel in recent coastal engineering projects [10] render the application of these theories for reliably estimating cusp spacing challenging and unreliable. According to the information recorded in Table 1, the methods employed in studies related to beach cusps include field observations, numerical modeling, sediment analysis, and laboratory investigations, each possessing distinct disadvantages despite their considerable advantages.

Table 1. Some of the most important theories about the formation and evolution of beach cusps

#	Theory	Researchers	Mechanism of cusp formation	Cusp Spacing Formula	Methods Used
1	Standing Edge Wave Theory	Guza and Inman (1975)	Cusps form due to the interaction between incoming waves and standing edge waves. The spacing is proportional to the wavelength of the edge waves	$\lambda_c = \frac{mg}{\pi} T^2 \sin\beta$ m is equal to 1 and 0.5 for subharmonic and synchronous edge waves, β is the beach slope, g is the acceleration due to gravity, and T is the wave period	Field Surveys, Numerical Modeling
2	Self-Organization Theory	Werner and Fink (1993)	Cusps emerge through a feedback mechanism involving sediment transport and wave run-up	$\lambda_c = fS_c$ S_c is the swash excursion across the beach and f is equal to 1.7	Field Surveys, Theoretical Modeling
3	Sanamura's Theory	Sanamura (2004)	Cusps form based on the relationship between the path of divergent uprush flow on horns and the cusp spacing, influenced by grain size of sediments.	$\lambda_c = A\varphi T\sqrt{gh}$ λ_c is cusp spacing, H is the nearshore wave height, T is the wave period, φ is a dimensionless quantity that shows the effect of the sediment grain size, and A is a constant estimated to be equal to 1.35	Field Surveys, Numerical Modeling, Sediment Analysis
4	Resonance Theory	Guza and Bowen (1976)	Beach cusps form when incoming wave frequencies resonate with natural modes of the beach morphology.	–	Field Surveys, Theoretical Analysis
5	Hydrodynamic Instability Theory	Coco, Huntley & O'Hare (2000)	Beach cusps result from instabilities in the wave and current interactions on the beach face, leading to rhythmic sedimentation patterns.	–	Numerical Modeling, Laboratory Experiments, Field Surveys

Field observations through direct method application, like GPS and terrestrial vehicles for measuring the characteristics of beach cusps entail a lot of profiles to adequately capture their morphology. Because these features are typically rhythmic, fieldwork takes a lot of time and labor [11][12][13][14][4]. In the same way, even with several hydrodynamic parameters estimated and changes in coastal morphology possible to study, numerical methods will still impose constraints on results being dependent on assumptions of the model. Such results would also have to be calibrated with computational resources drawn from field observations [8]. On the other hand, simplifications of some coastal processes are made by a researcher when it comes to numerical applications, yet modeling it truly in actuality is much complicated [15][16]. This method has also been used by researchers in studying the formation mechanisms of beach cusps [17][18].

The controlled conditions of laboratory methods provide accurate manipulation of variables affecting cusp spacing; however, results obtained from such methods do not hold in larger scales or extrapolate well into varying heterogeneous scales. While the monitoring of parameters related to beach cusps using remote sensing tools such as drones allows for the survey of a wide expanse of the beach face, offering significant advantages like spatial resolution, accuracy, and repeatability in monitoring compared to traditional methods [19], they are also employed as supplementary methods and are costly [20][21].Therefore, in the

investigation of features like beach cusps, due to their highly dynamic behavior and the absence of a cost-effective method, the utilization of tools such as various Artificial Intelligence (AI) models in conjunction with video-based techniques for observing morphological changes in the beach face and predicting the behavior of beach cusp systems can be highly efficient. Among different AI techniques, Artificial Neural Networks (ANNs), through their ability to estimate various quantities without the need for their direct measurement, are capable of solving a large number of scientific and engineering problems, including those related to coastal/ocean engineering [22].

To date, various studies have been conducted by researchers in this field to investigate coastal features using neural networks. Among these, the long-term prediction of sandbar behavior on coastlines using neural networks stands out [23]. Additionally, the most recent research undertaken by the authors of this paper focused on predicting beach cusp spacing based on neural network analysis, the results of which are used in the present study for comparison [24]. Several key factors motivated the authors' choice of the Adaptive Neuro-Fuzzy Inference System (ANFIS) for predicting beach cusp spacing. One key advantage is the combination of the capabilities of neural networks and fuzzy logic. As ANFIS is a unique hybrid technique integrating both Fuzzy Inference Systems (FIS) and Artificial Neural Networks (ANNs), it can simultaneously leverage the strengths of both systems [25][26]. Therefore, given that coastal phenomena such as the formation of multi-barred crescentic beach cusps often involve data with ambiguity, noise, or sometimes uncertainty, ANFIS, with its fuzzy rules and learning ability, can manage these complexities more effectively than purely neural models. Another rationale for having chosen the ANFIS for the prediction of beach cusp spacing lies in the non-linear and intricate behavior of beach cusps. ANFIS is capable of good performance when modeling nonlinear relationships and extracting fuzzy rules from data, and therefore it can better model the hidden relationships between input-output features.

The Adaptive Neuro-Fuzzy Inference System (ANFIS) further stands out for its enhanced interpretability when compared to 'pure' neural network systems. While classical neural models such as the Multilayer Perceptron (MLP) are commonly regarded as black, ANFIS is characterized by a high level of transparency and interpretability due to its usage of IF-THEN fuzzy rules; this is a distinct advantage for coastal analysts in analyzing geomorphological processes.

Furthermore, prior studies have demonstrated the considerable success of ANFIS in modeling marine phenomena and coastal morphological features [27][28][29][30]. Successful applications of this technique include predictions related to sea wave characteristics [28][31][32], wave run-up [33] , sea level forecasting [30][34][35][36][37], estimation of suspended sediment [38][39], and prediction of sediment transport rates [40]. Moreover, it is well-established that accessing large datasets can be challenging in coastal geomorphology studies, and ANFIS can effectively model even with limited but high-quality datasets. Consequently, the shortcomings of the aforementioned methods in studying coastal features, alongside the reasons outlined for choosing the ANFIS model, have prompted the authors to utilize ANFIS to smooth and bridge gaps in our overall understanding of cusp systems by estimating inter-cusp spacing and determining the morphological effects of swash on the beach face. The objectives of the present paper are as follows:

(a) Develop a robust ANFIS paradigm to estimate beach cusp spacing with a large dataset.

(b) Investigate this method with famous assessment methods regarding prediction quality.

(c) Compare the model performance with other soft computing methods, such as ANN, so the conclusion ends up with which of them gives better accuracy in prediction.

(d) Comparison of accuracy and performance for the best models in different sections of beach face. The remaining structure of this research has section 2 introducing materials and methods onto a discussion of the study area, datasets, and neuro-fuzzy model. This is followed by section 3 which discusses results obtained in ANFIS and neural network methods and analyzes those results. Finally, section 4 briefly summarizes all findings of this research.

2. Materials and Methods

This study developed an ANFIS architecture to obtain predictions for beach cusp spacing using morphodynamic datasets as input to the model. Initially, field observations made by Nuyts et al. (2021) were drawn out over different months as morphodynamic characteristics of the beach cusp system in different levels of the beach face [2][41].

Configurations concerning different ANFIS models are presented in Table 2. Then, statistical metrics relevant to each step were calculated, thus providing comparison grounds for the accuracy of the optimum configuration among competing membership functions at each elevation of the beach cusp system. Accordingly, sections of the coastline yielded the most acceptable output results. MATLAB Software (2019) was utilized in this study for the simulation of various models. With the help of an extensive toolbox, the software facilitates design and appraisal of models for the systems under investigation in this study. In the last phase, a comparison between results and numerical outputs published by Nuyts et al. (2021) also occurred.

Table 2. Different configurations of the ANFIS architectures

Type of Input MF	Number of MF	Number of Hidden Neurons	Type of Output MF	Number of Epochs	Learning Method
Pimf	3-3-3-3-3	-	Linear	50	hybrid
gauss2mf	3-3-3-3-3	-	Linear	50	hybrid
gaussmf	3-3-3-3-3	-	Linear	50	hybrid
trapmf	3-3-3-3-3	-	Linear	50	hybrid
psigmf	3-3-3-3-3	-	Linear	50	hybrid
gbellmf	3-3-3-3-3	-	Linear	50	hybrid
dsigmf	3-3-3-3-3	-	Linear	50	hybrid
trimf	3-3-3-3-3	-	Linear	50	hybrid

2.1. Description of the Study Area

Set against a shoreline of natural beauty and largely left undeveloped, Long Strand in Rosscarbery Bay is located in County Cork in the southwest of Ireland. Because of its unique geographical location to the North Atlantic Ocean, the area is being studied by specialists in coastal geomorphology, bed dynamics, and modeling of natural processes for its high dynamism concerning hydrodynamic conditions, geomorphological features, and oceanographic characteristics.

These coasts are associated with high-energy waves and strong littoral currents where the annual average significant wave height offshore is approximately 1.33m, with an annual mean period per wave of about 9.98 seconds. The prevailing winds also come from the southwest, by the way. In its natural biome morphologic characteristics, beach sand is darker and coarse-grained, median grain size (D_{50}) = 0.673 mm [42]. For Long Strand, as regards neap tide, it varies between 1.75m minimum and 1.7m standard maximum for spring tide, based on the Irish Transverse Mercator (ITM) grid, classifying it as a mesotidal beach.

Powerful ocean waves exposed this coast to highly dynamic sedimentary processes, rendering it an important site for investigating erosion and deposition. With beach cusps, features found between the high-water mark and the low-water mark, and bars below water level, this particular shoreline is typical among other sites along this coast [43][2] (Figure 2).

Figure 2. Satellite image of the study area (from Google Earth) (1) Upper level, (2) Middle level, and (3) Lower level of beach cusps [2]

2.2. Dataset

The surveys of a multi-level beach cusps system were employed during a field campaign using an Unmanned Aerial Vehicle (UAV) along the southwestern coast of Ireland between March and September 2019 [4]. Morphodynamic characteristics of the beach cusps system were recorded on 23 different days in a year, producing 61 morphodynamic datasets at various beach levels. These datasets were divided into four: cusp spacing (C_s), cusp elevation (C_e), cusp depth (C_d), and cusp amplitude (C_a). With regard to running ANFIS models, 80% of the data was allocated for training, while the rest 20% of the data was reserved for validating the predicted outcome [44]. Table 3 is a chart of some of the parameters of observed recorded beach cusps from field observations; Table 4 offers many statistical parameters related to the recorded data.

Table 3. Sample field observation data [2]

	Date	Level	Spacing(m)	Amplitude(m)	Elevation	Depth(m)
1	26 March	Upper Beach	39.5	0.86	5.41	16.91
		Mid Beach	38.5	0.58	3.14	16.57
		Low Beach	-	-	-	-
2	10 April	Upper Beach	40.3	0.83	5.46	15.01
		Mid Beach	24.6	0.34	2.81	12.31
		Low Beach	11.5	0.25	1.91	9.87
3	11 April	Upper Beach	39.2	0.87	5.62	14.98
		Mid Beach	25.0	0.43	2.76	12.69
		Low Beach	-	-	-	-
4	01 May	Upper Beach	38.9	1.05	4.87	15.67
		Mid Beach	14.9	0.21	2.33	9.06
		Low Beach	11.6	0.32	2.08	6.01
5	03 May	Upper Beach	37.7	0.81	5.69	13.24
		Mid Beach	12.8	0.23	2.42	8.81
		Low Beach	12.3	0.04	1.03	2.73
6	10 May	Upper Beach	37.9	0.79	5.68	12.32
		Mid Beach	19.9	0.29	2.96	8.55
		Low Beach	16.5	0.18	1.82	8.97

Table 4. Statistical parameters of recorded data [2]

Statistical properties	Upper Beach	Mid Beach	Low Beach
Max (m)	40.9	38.5	16.7
Min (m)	37.7	11.1	6.5
Mean (m)	40.26	18.17	11.09
Standard Deviation (m)	0.95	5.48	2.91
Coefficient of Variation	0.02	0.30	0.26

2.3. ANFIS Neuro-Fuzzy Model

The ANFIS neuro-fuzzy system is an intelligent hybrid model that is structured like a multilayer perceptron feedforward neural network designed by integrating artificial neural network learning algorithms with fuzzy inference systems. The first introduction was made by Jang (1993), and the proposed model is based on the Takagi-Sugeno fuzzy system rules. [25].

Within the architecture of this network, the nonlinear mapping of the input space into the output space is established through IF-THEN rules. Each rule output is designed as a linear combination of the input variables plus one constant, and the final output is the weighted average of the outputs of all the rules. Relations for the IF-THEN rules of a Takagi-Sugeno system with three inputs are given as follows:

Rule 1: IF x is A_1 and y is B_1 and z is C_1 THEN $f_1 = p_1x + q_1y + r_1z + s_1$ (1)

Rule 2: IF x is A_2 and y is B_2 and z is C_2 THEN $f_2 = p_2x + q_2y + r_2z + s_2$ (2)

Rule 3: IF x is A_3 and y is B_3 and z is C_3 THEN $f_3 = p_3x + q_3y + r_3z + s_3$ (3)

B_i, A_i, and C_i would be the membership functions for inputs x, y, and z, respectively, while p_i, q_i, and r_i would be the parameters of the output function, and s_i would be a constant. This output value y* would be inferred by some relations.

$$y^* = f = \frac{(w_1 f_1 + w_2 f_2 + w_3 f_3)}{w_1 + w_2 + w_3} = \overline{w_1} f_1 + \overline{w_2} f_2 + \overline{w_3} f_3 \quad (4)$$

The ANFIS architecture consists of five layers, each of which has specific functions (Figure 3). The first and the fuzzification layer transforms x, y, and z into membership degrees via A_1, B_1, and C_1 for the first fuzzy rule, A_2, B_2, and C_2 for the second fuzzy rule, and A_3, B_3, and C_3 for the third fuzzy rule. The second layer is the rule layer, which combines the membership values in the antecedent part to obtain the weight of each rule. The third layer, known as the weight's normalization layer, calculates the normalized weight by dividing the weight of each rule by the sum of the weights of all possible rules, denoted as w_1, w_2, and w3 for rules 1, 2, and 3, respectively. The output of each rule that is obtained by multiplying the weight and the output defined in the consequent part of the fuzzy rule is calculated in the fourth layer or the defuzzification layer. The overall output in this part (output layer) is determined and recorded as the sum of all outputs from the fuzzy rules [28].

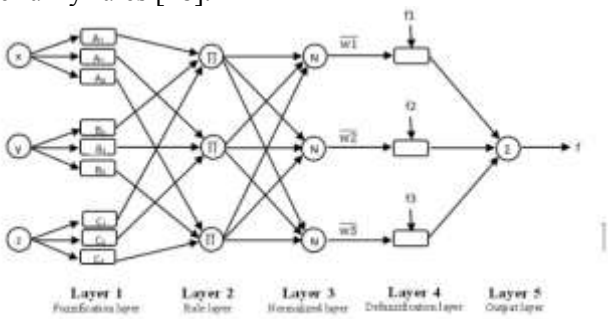

Figure 3. The structure of ANFIS model.

2.4. Evaluation Criteria

Different models are ordinarily assessed by calculating the discrepancies between the predicted and the observed values based on five statistical parameters. These parameters include the Coefficient of Efficiency (CE), Correlation Coefficient (R), Root Mean Square Error (RMSE), the Scatter Index (SI), and Mean Square Error (MSE), defined in Equations 5-9.

$$CE = 1 - \frac{\sum_{i=1}^{N}(O_i - P_i)^2}{\sum_{i=1}^{N}(O_i - \bar{O}_m)^2} \quad (5)$$

$$R = \frac{\sum_{i=1}^{N}(O_i - \bar{O}_m)\sum_{i=1}^{N}(P_i - \bar{P}_m)}{\sqrt{\sum_{i=1}^{N}(O_i - \bar{O}_m)^2}\sqrt{\sum_{i=1}^{N}(P_i - \bar{P}_m)^2}} \quad (6)$$

$$RMSE = \sqrt{\frac{1}{N}\sum_{i=1}^{N}(P_i - O_i)^2} \quad (7)$$

$$SI = \frac{RMSE}{\text{avrage observed value}} \quad (8)$$

$$MSE = \frac{1}{N}\sum_{i=1}^{N}(P_i - O_i)^2 \quad (9)$$

Here, N represents the total number of data points, O_i is the observed value obtained from field studies, $P_i$is the predicted value from the model results, $\bar{O}_m$ denotes the mean of the observed values from field studies, and $\bar{P}_m$is the mean of the predicted values calculated from the model results.

The range of Coefficient of Efficiency (CE) is one of the evaluation criteria by which values closer to one are regarded as a more ideal model [42]. The value of Correlation Coefficient (R) lies always between -1 and 1; the value 1 indicates zero error in prediction. RMSE usually is a popular parameter used to evaluate models that assume the errors follow a normal distribution. The RMSE value coming closer toward zero would indicate a higher accuracy in prediction [43]. The Scatter Index (SI) is also the percentage of the predicted data from the actual data in terms of dispersion, wherein 0 would mean that there is no dispersion in the model's prediction output. Another evaluation parameter is the range of the Coefficient of Efficiency (CE); a value of this metric closest to one will then indicate an ideal model [44].

3. Discussion and Conclusion

3.1. ANFIS Model Results

In this study, ANFIS was employed with the aim of accurately and interpretably modeling the relationships among geometric parameters. The results obtained from implementing this model demonstrated that selecting an appropriate structure for fuzzy rules and membership functions plays a key role in enhancing the model's accuracy and generalizability. Visual evaluation of the model through the Rule Viewer and analysis of the initial membership functions provided greater transparency regarding the model's operation and sensitivity to input variations. Figure 4 presents a view of the ANFIS Rule Viewer, illustrating the performance of 27 fuzzy rules in response to three input parameters- cusp depth (C_d), cusp elevation (C_e), and cusp amplitude (C_a)-and one output (Cusp spacing). Each column represents one of the input parameters, and the yellow lines indicate the activation level of each rule for the current input value (shown by the red line). The final column displays the output of each rule using blue rectangles.

As shown in this figure, for the current input values (Depth=9.05, Elevation=3.38, Amplitude=0.445), the highest activation corresponds to the intermediate rules, which match the "Medium" levels of the input membership functions. This indicates that the model assigns greater weight to the intermediate rules, and the final output (Cusp spacing=33) is determined accordingly. Such behavior demonstrates the model's accuracy and efficiency in appropriately identifying and weighting fuzzy rules under real data conditions.

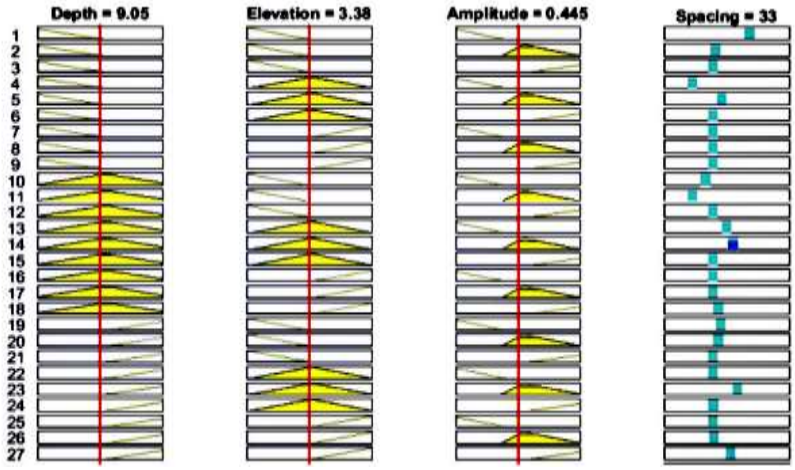

Figure 4. Rule viewer of designed fuzzy model.

The functional structure of ANFIS model for two types of input initial membership functions for input parameters (depth, elevation, and amplitude) is depicted in Figure 5. Upper sections (a, b, c) show the model using trimf membership function; lower sections illustrate the functional operation of the model under the pimf membership function. Each input parameter is divided into three fuzzy sets labeled "Low," "Medium," and "High," which each decide the degree of membership for the input value. Within (d), a 3D illustration depicts the relationships between the input variables (Elevation vs Depth shown in the upper graph; Amplitude vs Elevation shown in the lower graph) and the output variable (Cusp spacing). The three-dimensional surfaces therefore denote the complex non-linear interdependencies between input and output parameters; thus, proving ANFIS's strength in identifying hidden patterns within the data. Trimf and pimf membership functions differ in transition behavior; trimf has clear boundaries and linear transition, while pimf transition is smooth and floored with overlapping characteristics, increasing model flexibility in dealing with real-life data. The different slopes observed in the 3D surfaces indicate the response of the model output to changes in input parameters, which is important for further analyses and finding critical points in the system.

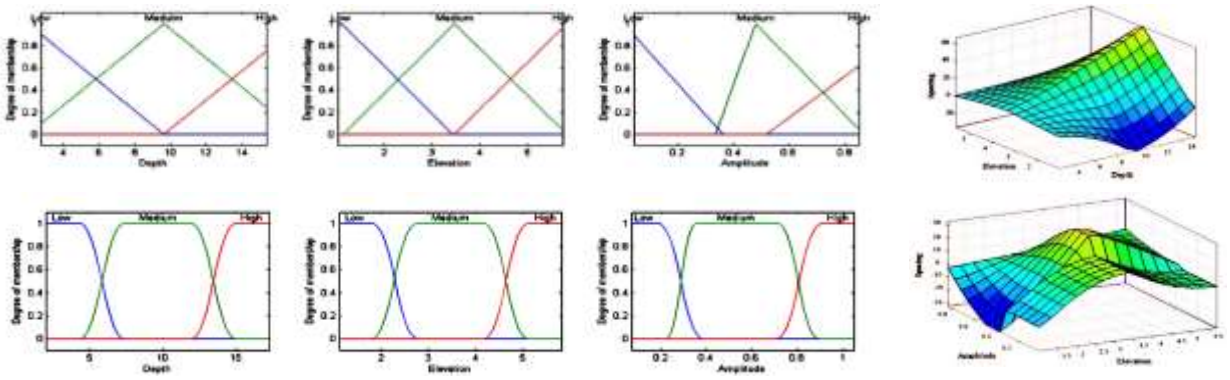

(a) (b) (c) (d)

Figure 5. Two examples of the initial membership functions (trimf and pimf) of X-axis input parameters for the ANFIS model: (a) Depth (b) Elevation, (c) Amplitude (d) 3D surface visualization of the relationship between the input and spacing cusps.

The ANFIS model performances are listed in the tables of statistical metrics achieved for all the phases of identification (Table 5). Since Model (VIII) stated in the table provides better accuracy from training and testing phases compared to the other models as shown by various metrics, therefore, this model is found to be better in fitting the data. R is the metric that indicates how well the predicted values correlate with the actual values; the closer R is to 1, the better the model has performed, exhibiting a high degree of consistency in prediction with the actual data.

From the bar chart shown in Figure (6a), R for the model with 'trimf' membership functions is significantly higher for both training and testing, therefore, indicating that the data was fit more by this model. The RMSE signifies the absolute error in prediction, with lower values implying higher model fitness. The model with the 'trimf' function has shown the lowest RMSE in both training and testing phases as shown in the bar chart in Figure (6b). So, this contributes to lower errors and more accurate predictions when compared with other models. The combination of these two ranges hence would argue that the ANFIS with the 'trimf' function achieved a robust trade-off between accuracy and error in predicting the data. This becomes very important as in practical scenarios the models that are less erroneous as well as highly correlated to the actual data are more acceptable. In addition, the difference between the performances of the models during training and testing suggests generalization strength of the model 'trimf' one is a good performer even in testing and hence is free from overfitting and predicting fresh data.

The main outcome of Figure 6 suggests the ANFIS model with the 'trimf' membership function to be excellent for prediction for this study, as it had the highest R value (very close to 1) in conjunction with the lowest RMSE value during both testing and training phases. Hence, implying the highest prediction accuracy and stability for new data. The 'dsigmf' and 'psigmf' models, on the contrary, got low ratings and high RMSE, which means they were not capable of learning and generalizing to new data. Further, variations in model performance between training and testing in some instances indicate their sensitivity and instability against the input data.

Table 5. Results of different models of ANFIS

Archite-cture. no	Type of MFs		Phases	RMSE	MSE	SI	CE	R	Overall (MSE)
	Input	Output							
I	pimf	Linear	Training	0.047321	0.002239	0.001782	0.999987	0.997739	0.001881
			Testing	0.020456	4.18E-04	0.001177	0.999994	0.99916	
II	gauss2mf	Linear	Training	0.05265	0.002772	0.001983	0.999984	0.998475	0.002298
			Testing	0.019052	3.63E-04	0.001096	0.999995	0.998209	
III	gaussmf	Linear	Training	0.077447	0.005998	0.002917	0.999965	0.996026	0.004932
			Testing	0.024149	5.83E-04	0.00139	0.999992	0.99948	
IV	trapmf	Linear	Training	0.052437	0.00275	0.001975	0.999984	0.998714	0.002302
			Testing	0.02179	4.75E-04	0.001254	0.999993	0.998719	
V	psigmf	Linear	Training	0.06841	0.00468	0.002577	0.999973	0.997655	0.003954
			Testing	0.031501	9.92E-04	0.001813	0.999986	0.999859	
VI	gbellmf	Linear	Training	0.052679	0.002775	0.001984	0.999984	0.998773	0.002314
			Testing	0.020873	4.36E-04	0.001201	0.999994	0.999591	
VII	dsigmf	Linear	Training	0.068128	0.004641	0.002566	0.999973	0.998809	0.004037
			Testing	0.039644	0.001572	0.002282	0.999978	0.998488	
VIII	trimf	Linear	Training	0.037968	0.001442	0.00143	0.999992	0.9999	0.001192
			Testing	0.013254	1.76E-04	7.63E-04	0.999998	0.9999	

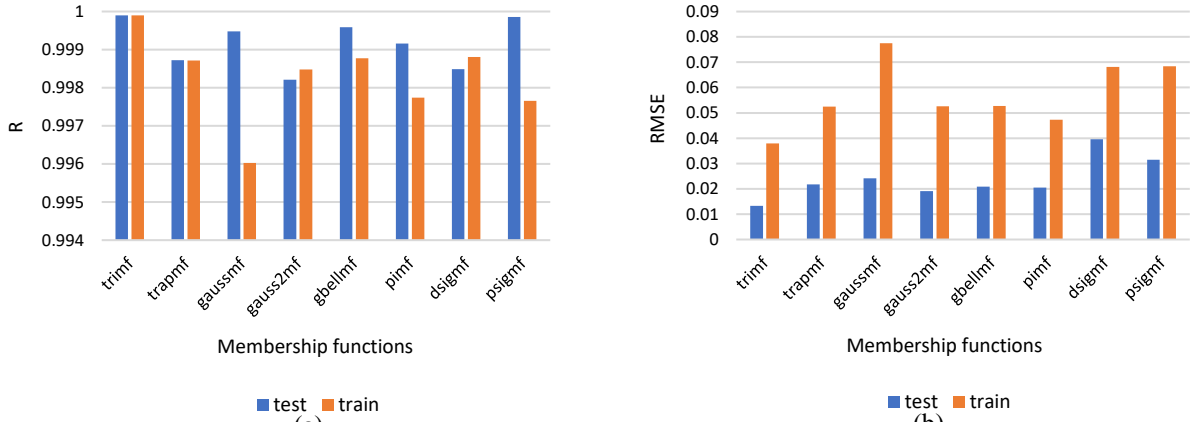

Figure 6. Variation of (a) R and (b) RMSE for ANFIS models

Figure 7 presents box plots concerning percentage error for different ANFIS models in two phases: testing (Figure 7a) and training (Figure 7b). The examination of these plots tells us that the line within each box indicates the median value (second quartile); the cross symbol indicates the mean of the data; and the box width indicates the interval between the first and third quartiles, that is, the IQR. The purpose of this figure, aside from rating the models' accuracies, is to rate their stability and sensitivity to input data.

A comparison of the box plots validates that in the testing phase, the error percentage is quite variable for the dsigmf model, exhibiting the largest IQR, signifying the model is input data-sensitive and unstable. In addition, the model possesses outliers, suggesting instances where error values are dramatically larger than normal. During the training phase, the gbellmf, dsigmf, and psigmf models also show high IQRs, which means their errors are also very dispersed. In contrast, the models with the smallest IQRs during both the testing and training phase are the trimf, which indicates a very limited range of variability in percentage error, and is one in which most of the errors are near its central value. This model also has the least median and mean error values as compared to all other tested models, and its box plot is nearly symmetrical, with median and mean being almost coincident. There are no significant amounts of outliers in this model and it shows the most consistent and reliable performance across all data instances.

The ANFIS model with the trimf membership function is the best among all membership functions examined in terms of error magnitude, error dispersion and the presence of outliers, which figure 7 demonstrates very well. This overarching superiority suggests that the trimf model is both stable and accurate in prediction compared to others.

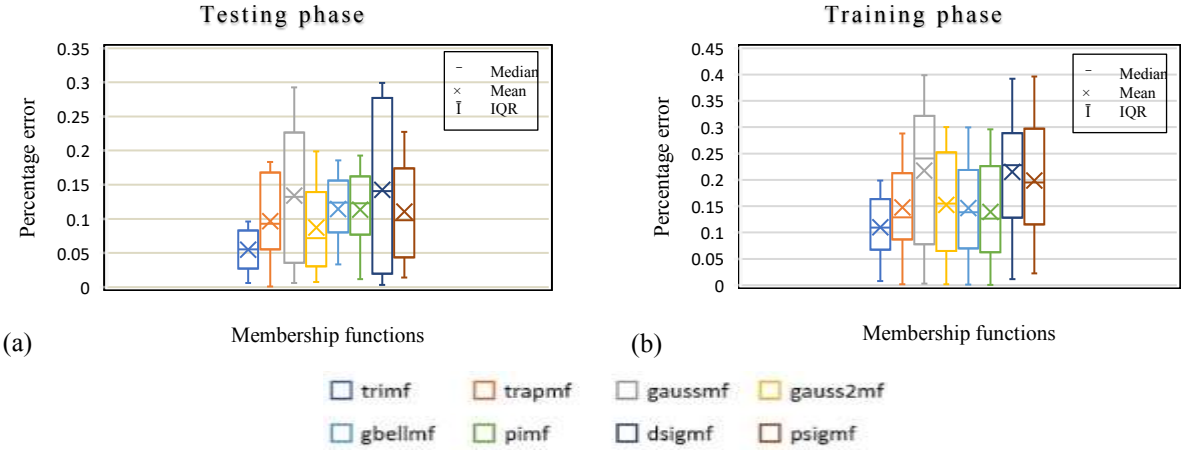

Figure 7. Box plots of percentage error for ANFIS models (a) testing and (b) training stage.

The evaluated ANFIS model with the trimf membership function presents a comparison between the observed and predicted data of beach cusp spacing in training (a) and testing (b) (Figure 8). The blue dotted lines represent actual data, while red dotted lines are predicted data. The close agreement of both data sets in both phases considered with even lower MSE values (0.0014416 in training and 0.00017567 in testing) indicates a very high accuracy of the model in reproducing and predicting the complex trends of cusp spacing. This, thus, confirms the generalization capability and reliable performance in real-world conditions and unseen data for ANFIS (trimf) model.

Radar plots (spider plots) are made on the five statistical measures called the correlation coefficient (R), the root mean squared error (RMSE) and the mean

square error (MSE), the index of agreement (SI), and the efficiency coefficient (CE) to evaluate the performance of ANFIS in the model with different membership functions for their predictions on cusp spacing in training (a) and testing (b) phases. Such plots can facilitate easy comparisons of model performance across different facets.

In the stage of training (Figure 9a), gaussmf is the membership function for which the model gives the worst performance among these models; in most of the metrics, this model's values were less favorable than those of every other model. This is quite extreme in the RMSE and MSE metrics, where this model indicated a higher value. Meanwhile, the trimf model had exhibited better performance through most of the metrics, issuing favorable values.

In the testing phase (Figure 9b), the dsigmf model exhibits the lowest accuracy in most of the statistical measures clearly deviating from the other models. It then has higher values in RMSE and MSE but shows poor performance in CE and R metrics. Hence, it indicates high sensitivity and instability of the dsigmf model when faced with new and unseen data.

As observed in Figure 9, ANFIS model used with the trimf membership function revealed superior performance values in the majority of statistical metrics during both the training and the testing phases. It is important to note that in the final evaluation and selection of the best model, the criteria of the correlation coefficient (R) and the mean square error (MSE) were emphasized the most, as these two metrics really represent the accuracy and generalization capability of the model. Hence, best performance was given to the trimf model, which finally gets selected as the best model.

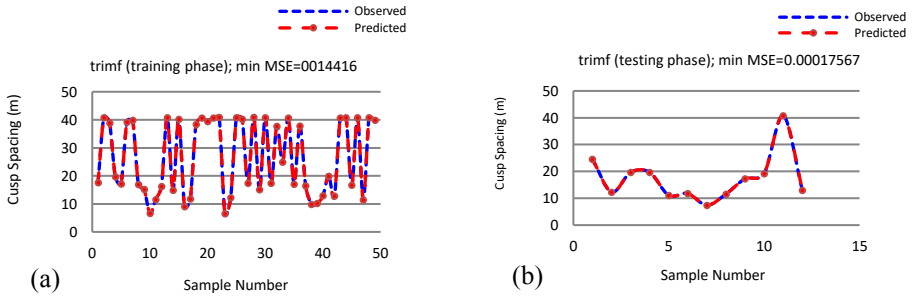

Figure 8. Compare the observed cusp spacing and the best predicted performance of optimal model-ANFIS (trimf), a) Training phase b) Testing stage.

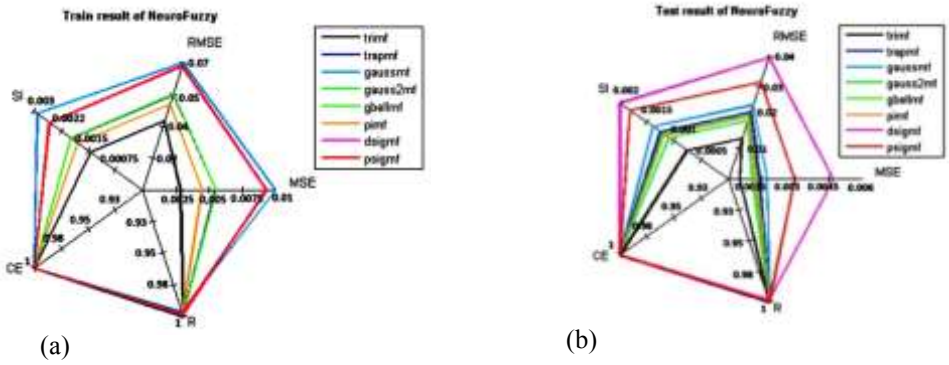

Figure 9. Spider plots of five performance criteria for prediction of cusp spacing in a) training and b) testing stages.

Figure 10 consists of three scatter plots showing the relationship between predicted cusp spacing by the optimized ANFIS model with the trimf membership function and the beach cusps' three primary morphological parameters: Amplitude, Elevation, and Depth. All plots show the relationship between the parameters investigated, including the linear regression line and coefficient of determination (R^2) reflecting the strength of correlation between the variables.

Plot (a) considers the relationship between cusp spacing and cusp amplitude. The R^2 value of 0.86 confirms a strong correlation between these two parameters, signifying that changes in cusp spacing are significantly associated with changes in their amplitude. The slope of the regression line (0.0209) further asserts that an increase in cusp spacing results in an increase in amplitude in direct proportion to it. In plot (b), the focus is on the relationship between cusp spacing and cusp elevation. The R^2 value for this plot is calculated to be 0.90, signifying a very high and significant correlation between these two parameters. This is the highest coefficient of determination among the three plots and infers that cusp spacing greatly influences the elevation of cusps. The slope of the line of regression is 0.1248, indicating that with an increase in cusp spacing, elevation also increases greatly. Plot

(c) gives the relationship between cusp spacing and depth. The R^2 value for this plot is 0.70, indicating a moderate correlation between these two parameters. Though a positive and linear correlation exists with a slope of 0.262 for cusp spacing to depth, the data points here show greater dispersion compared to the previous two plots, indicating that some other factors may also influence the depth of cusps. These three plots together affirm that the ANFIS model with the trimf membership function successfully drew reasonably strong linear correlations between cusp spacing and their primary morphological parameters. More significantly, the higher R^2 value in the elevation plot, compared with that of amplitude and depth, puts additional emphasis on the importance of elevation with respect to cusp spacing. Equally, the positive slopes of the regression lines trending in all three plots assist in inferring that in addition to cusp spacing, other morphological parameters also tend to increase in direct proportion with it.

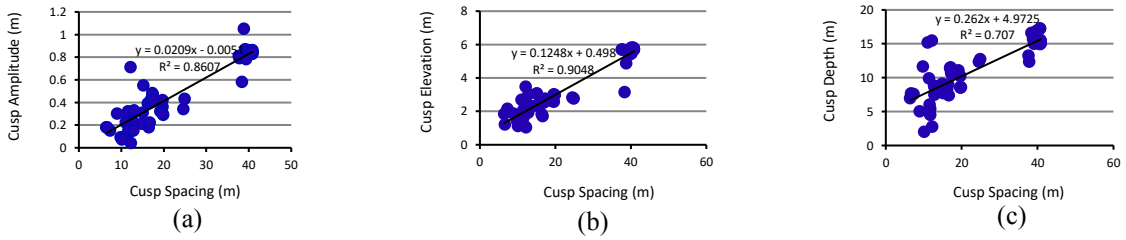

Figure 10. Scatter plots of the predicted cusp spacing versus other parameters of the cusps, based on the ANFIS (trimf) model, (a)cusp amplitude, (b) cusp elevation, and (c) cusp depth

3.2. Comparison Between ANN and ANFIS

Figure 11 shows box plots of relative error in the beach face for three sections - Upper, Mid, and Low sections of the beach face with respect to the ANFIS (trimf) model. Obviously, the central line in the box will represent the median error in that box, while the symbol × indicates the value of the mean error. Furthermore, a boxwidth indicates the interquartile range (IQR) of the data. It is evident that the lowest mean relative error occurs in the Mid Beach section of the ANFIS (trimf) model. The lowest median relative error was recorded in the Low section; this implies that these two zones exhibit the same behavior with respect to beach cusp spacing prediction, in which the model's performance is better and more consistent than in most Upper beach sections. Furthermore, the dispersions of errors occurring in the Low section of the beach face are smaller compared with other sections, which indicates a higher stability and robustness of the model in that area. This will become practically important, as the model has actually been performing more reliably for those parts of the beach face experiencing considerable morphological adjustment.

Taking into account that the authors have employed artificial neural networks in some studies to assess the variations that happen in cusp spacings [24], this study will therefore aim at assessing the ANFIS model's performance through comparing the obtained MSE values from both methods and in turn improve on the investigation into the predictive metrics of each of the models as well as the groundworks for providing better discussions on the performances and generalization capabilities of the various models in predicting morphodynamic patterns throughout some regions of the beach face.

Figure 12 provides the MSE values of various ANN and ANFIS models in bar chart form, as well as in tabular format, across the beach face sections. These values are compared and it was found that the ANFIS (trimf) model always gave the lowest MSE as compared with the three fished out ANN models (ANN with CFBP, FFBP, and EBP algorithms) across the entire beach face sections. Specifically, the least MSE among all sections and models was recorded for the ANFIS model in the Low Beach Face section, scoring a net value of 0.0001. On the flip side, the least MSE values for the ANN types are predominantly seen under the Upper Beach Face section (specifically under ANN (EBP) model with a value of 0.06).

It is worth noting that ANFIS (trimf) model performs very well in all other sections and not just in Low Beach Face section, with MSE scores greatly lower than those recorded by ANN models. Hence, this buttresses the claim that the ANFIS model has a higher competence in simulating and forecasting spacings between beach cusps in Low Beach Face region, which usually has more complex conditions from morphodynamics.

In summary, the conclusion derived from this is that artificial neural network models were quite acceptable for application on the Upper Beach Face section, while there was a clear difference between the two models with the ANFIS (trimf) being much preferable in terms of accuracy and stability, primarily in Mid Beach Face and Low Beach Face. Consequently, the ANFIS (trimf) model is recommended for more precise simulation and prediction of morphodynamic features in lower beach face areas, while ANN models could be more suitable for upper beach face areas. This critical comparison indicates the preference for selecting the finest model for the conditions or characteristics of each section of beach face.

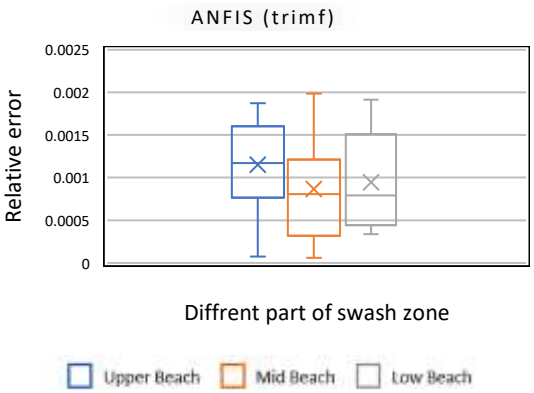

Figure 11. Box plots of relative error in different parts of the beach face in ANFIS (timf) model.

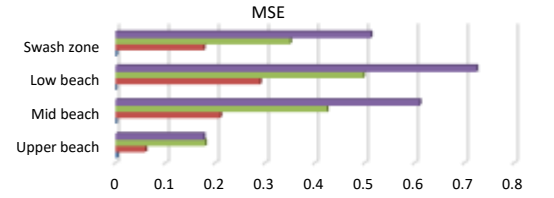

	Upper beach	Mid beach	Low beach	Swash zone
ANN (CFBP)	0.1769	0.61	0.7243	0.512
ANN (FFBP)	0.1798	0.424	0.4972	0.3502
ANN (EBP)	0.06	0.21	0.2897	0.1769
ANFIS (trimf)	0.0025	0.0005	0.0001	0.001

Figure 12. The magnitudes of MSE of optimal models in different parts of the beach and different models.

4. Results

The study adopted the Adaptive Neuro-Fuzzy Inference System (ANFIS) model for the prediction of the spacing of multi-barred crescentic beach cusps. The results obtained from this model showed that correctly choosing a fuzzy rule structure and membership functions was instrumental in enhancing the model's accuracy and interpretability. The analysis of the model performance using the Rule Viewer and initial membership function examination added much transparency related to the way model output varies concerning input changes.

The ANFIS model using the triangular membership function (trimf) performed best in this study compared to other models tested in both training and test phases. The model exhibited a high correlation coefficient (R close to 1); low values for Root Mean Square Error (RMSE) and Mean Square Error (MSE); and very low dispersion of errors (low IQR). Moreover, the absence of outliers in the trimf model output indicates the stability and reliability of this model in the face of new data.

The results from the comparison made between the ANFIS model and optimal ANN models considered for this study also indicated that the ANFIS (trimf) achieved higher prediction accuracy and significantly lower error values than the ANN models in all the different beach face zones (Upper Beach Face, Mid Beach Face, and Low Beach Face). In particular, in the Low Beach Face area, the ANFIS model exhibited superior performance by recording the lowest MSE value.

When the relationships between the beach cusp spacing and three morphological parameters-amplitude, elevation, and depth of the beach cusps-were examined, strong and significant ones were extracted by the model, with the highest correlation being found between the spacing and the elevation of the beach cusps (R^2=0.9).

In summary, the current study concluded high spatial accuracy, good generalization capability, stability, and enhanced interpretability of the proposed ANFIS with trimf membership function as a promising technique for predicting the spacing of multi-barred crescentic beach cusps, thus placing it in the front line when compared to optimal ANN models.

5. References

1. Ribas, F., Falqués, A., Deèswart, H. E., Dodd, N., Garnier, R., & Calvete, D. (2015). Understanding coastal morphodynamic patterns from depth-averaged sediment concentration. *Reviews of Geophysics*, *53*(2), 362–410. https://doi.org/10.1002/2014RG000457

2. Nuyts, S., Li, Z., Hickey, K., & Murphy, J. (2021). Field observations of a multilevel beach cusp system and their swash zone dynamics. *Geosciences (Switzerland)*, *11*(4), 1–24. https://doi.org/10.3390/geosciences11040148

3. Vousdoukas, M. I. (2012). Characteristics and interactions of multiple beach cusp systems on a meso-tidal, steeply-sloping beach. *Proceedings of the International Offshore and Polar Engineering Conference*, *4*, 1475–1481.

4. Nolan, T. J., Kirk, R. M., & Shulmeister, J. (1999). Beach cusp morphology on sand and mixed sand and gravel beaches, South Island, New Zealand. *Marine Geology*, *157*(3–4), 185–198. https://doi.org/10.1016/S0025-3227(98)00150-9

5. Guza, R.T. and Inman, D. (1975). Edge Waves and Beach Cusps. *Journal of Geophysical Research*, *80*(21), 2997–3012. https://doi.org/10.9753/icce.v16.81

6. Guza, R. T., & Bowen, A. J. (1976). Finite Amplitude Edge Waves. *Journal of Marine Research*, *34*(2), 269–293.

7. Werner, B. T., & Fink, T. M. (1993). Beach cusps as self-organized patterns. *Science*, *260*(5110), 968–971. https://doi.org/10.1126/science.260.5110.968

8. Sunamura, T. (2004). A predictive relationship for the spacing of beach cusps in nature. *Coastal Engineering*, *51*(8–9), 697–711.

https://doi.org/10.1016/j.coastaleng.2004.07.004
9. Coco, G., D. A. Huntley, and T. J. O. (2000). Investigation of a self-organisation model for beach cusp formation and development. *J. Geophys. Res*, *105–21*(1), 991– 22,002.
10. Guest, T. B., & Hay, A. E. (2019). Timescales of beach cusp evolution on a steep, megatidal, mixed sand-gravel beach. *Marine Geology*, *416*(September 2018), 105984.
11. Ali, S., Darsan, J., & Wilson, M. (2017). Cusp morphodynamics in a micro-tidal exposed beach. *Journal of Coastal Conservation*, *21*(6), 777–788. https://doi.org/10.1007/s11852-017-0536-2
12. Shiea-Ali, M., & Valipour, A. (2021). Impact of Hydrodynamic Forces on Morphodynamic Classification of Beaches in some parts of the Iranian coasts. International Journal of Coastal and Offshore Engineering, 5(3), 26–39. https://doi.org/10.52547/ijcoe.5.3.26
13. Masselink, G. (1999). Alongshore variation in beach cusp morphology in a coastal embayment. *Earth Surface Processes and Landforms*, *24*(4), 335–347. https://doi.org/10.1002/(sici)1096-9837(199904)24:4<335::aid-esp968>3.3.co;2-8
14. Pitman, S. J., Hart, D. E., & Katurji, M. H. (2019). Application of UAV techniques to expand beach research possibilities: A case study of coarse clastic beach cusps. *Continental Shelf Research*, *184*(July), 44–53. https://doi.org/10.1016/j.csr.2019.07.008
15. Sathish, S., Kankara, R. S., & Rasheed, K. (2018). Morphometric and sediment analysis of beach cusp in correlation to rip currents: a case study from tropical coast, West coast of India. *Environmental Earth Sciences*, *77*(16), 0. https://doi.org/10.1007/s12665-018-7754-2
16. Daly, C. J., Floc'h, F., Almeida, L. P. M., Almar, R., & Jaud, M. (2021). Morphodynamic modelling of beach cusp formation: The role of wave forcing and sediment composition. *Geomorphology*, *389*, 107798. https://doi.org/10.1016/j.geomorph.2021.107798
17. Kaneko, A. (1985). Formation of beach cusps in a wave tank. *Coastal Engineering*, *9*(1), 81–98. https://doi.org/10.1016/0378-3839(85)90028-6
18. Aoki, H., & Sunamura, T. (2000). A laboratory experiment on the formation and morphology of beach cusps. *Chikei*, *21*(3), 291–306.
19. Pitman, S. J., Coco, G., Hart, D. E., & Shulmeister, J. (2024). Observations of beach cusp morphodynamics on a composite beach. *Geomorphology, 447*, 109026. https://doi.org/10.1016/j.geomorph.2023.109026
20. Masselink, G., Hegge, B. J., & Pattiaratchi, C. B. (1997). Beach cusp morphodynamics. *Earth Surface Processes and Landforms, 22*(12), 1139–1155. https://doi.org/10.1002/(SICI)1096-9837(199712)22:12<1139::AID-ESP766>3.0.CO;2-1
21. Van Gaalen, J. F., Kruse, S. E., Coco, G., Collins, L., & Doering, T. (2011). Observations of beach cusp evolution at Melbourne Beach, Florida, USA. *Geomorphology, 129*(1–2), 131–140. https://doi.org/10.1016/j.geomorph.2011.01.019
22. Alexandridis, A. (2013). Evolving RBF neural networks for adaptive soft-sensor design. *International Journal of Neural Systems, 23*(6), 1–14. https://doi.org/10.1142/S0129065713500299
23. Pape, L., Ruessink, B. G., Wiering, M. A., & Turner, I. L. (2007). Recurrent neural network modeling of nearshore sandbar behavior. *Neural Networks, 20*(4), 509–518. https://doi.org/10.1016/j.neunet.2007.04.007
24. Valipour, A., & Shirgahi, H. (2024). Prediction of the multi-level beach cusp spacing using artificial neural networks. *Iranian Journal of Geophysics, 17*(5), 1–18. https://doi.org/10.30499/IJG.2023.387044.1500
25. Jang, J. S. R. (1993). ANFIS: Adaptive-network-based fuzzy inference system. *IEEE Transactions on Systems, Man, and Cybernetics, 23*(3), 665–685. https://doi.org/10.1109/21.256541
26. Brown, M., & Harris, C. (1995). *Neurofuzzy adaptive modeling and control*. Englewood Cliffs, NJ: Prentice-Hall.
27. Kisi, O. (2005). Suspended sediment estimation using neuro-fuzzy and neural network approaches. *Hydrological Sciences Journal, 50*(4), 683–696. https://doi.org/10.1623/hysj.2005.50.4.683
28. Kazeminezhad, M. H., Etemad-Shahidi, A., & Mousavi, S. J. (2005). Application of fuzzy inference system in the prediction of wave parameters. *Ocean Engineering, 32*(14–15), 1709–1725. https://doi.org/10.1016/j.oceaneng.2005.02.001
29. Hong, Y. S. T., & White, P. A. (2009). Hydrological modeling using a dynamic neuro-fuzzy system with on-line and local learning algorithm. *Advances in Water Resources, 32*(1),

110–119. https://doi.org/10.1016/j.advwatres.2008.10.006

30. Shiri, J., Makarynskyy, O., Kisi, O., Dierickx, W., & Fard, A. F. (2011). Prediction of short-term operational water levels using an adaptive neuro-fuzzy inference system. *Journal of Waterway, Port, Coastal, and Ocean Engineering, 137*(6), 344–354. https://doi.org/10.1061/(ASCE)WW.1943-5460.0000097

31. Özger, M. (2009). Neuro-fuzzy approach for the spatial estimation of ocean wave characteristics. *Advances in Engineering Software, 40*(9), 759–765. https://doi.org/10.1016/j.advengsoft.2009.02.004

32. Bozorgzadeh, L., Bakhtiari, M., Shani Karam Zadeh, N., & Esmaeeldoust, M. (2019). Forecasting of wind-wave height by using adaptive neuro-fuzzy inference system and decision tree. *Journal of Soft Computing in Civil Engineering, 3*(3), 22–36. https://doi.org/10.22115/scce.2019.199291.1125

33. Bakhtyar, R., Yeganeh Bakhtiary, A., & Ghaheri, A. (2008). Application of neuro-fuzzy approach in prediction of runup in swash zone. *Applied Ocean Research, 30*(1), 17–27. https://doi.org/10.1016/j.apor.2008.02.004

34. Lin, L. C., & Chang, H. K. (2008). An adaptive neuro-fuzzy inference system for sea level prediction considering tide-generating forces and oceanic thermal expansion. *Terrestrial, Atmospheric and Oceanic Sciences, 19*(1–2), 163–172. https://doi.org/10.3319/TAO.2008.19.1-2.163(SA)

35. Karimi, S., Kisi, O., Shiri, J., & Makarynskyy, O. (2013). Neuro-fuzzy and neural network techniques for forecasting sea level in Darwin Harbor, Australia. *Computers & Geosciences, 52*, 50–59. https://doi.org/10.1016/j.cageo.2012.09.015

36. Kaloop, M. R., El-Diasty, M., & Hu, J. W. (2017). Real-time prediction of water level change using adaptive neuro-fuzzy inference system. *Geomatics, Natural Hazards and Risk, 8*(2), 1320–1332. https://doi.org/10.1080/19475705.2017.1327464

37. Wang, B., Wang, B., Wu, W., Xi, C., & Wang, J. (2020). Sea-water-level prediction via combined wavelet decomposition, neuro-fuzzy and neural networks using SLA and wind information. *Acta Oceanologica Sinica, 39*(5), 157–167. https://doi.org/10.1007/s13131-020-1569-1

38. Kisi, O., Haktanir, T., Ardiclioglu, M., Ozturk, O., Yalcin, E., & Uludag, S. (2009). Adaptive neuro-fuzzy computing technique for suspended sediment estimation. *Advances in Engineering Software, 40*(6), 438–444. https://doi.org/10.1016/j.advengsoft.2008.06.004

39. Shamaei, E., & Kaedi, M. (2016). Suspended sediment concentration estimation by stacking the genetic programming and neuro-fuzzy predictions. *Applied Soft Computing, 45*, 187–196. https://doi.org/10.1016/j.asoc.2016.03.009

40. Sadeghifar, T., & Barati, R. (2018). Application of adaptive neuro-fuzzy inference system to estimate alongshore sediment transport rate (a real case study: Southern shorelines of Caspian Sea). *Journal of Soft Computing in Civil Engineering, 2*(4), 72–85. https://doi.org/10.22115/SCCE.2018.135975.1074

41. Nuyts, S., Murphy, J., Li, Z., & Hickey, K. (2020). A methodology to assess the morphological change of a multilevel beach cusp system and their hydrodynamics: Case study of Long Strand, Ireland. *Journal of Coastal Research, 95*(sp1), 593–598. https://doi.org/10.2112/SI95-116.1

42. Ruz, M. H. (1989). Recent evolution of the southeast barrier coast of Ireland. *Journal of Coastal Research, 5*(3), 523–539.

43. Malvarez, G. C., Cooper, J. A. G., & Jackson, D. W. T. (2001). Relationships between wave-induced currents and sediment grain size on a sandy tidal-flat. *Journal of Sedimentary Research, 71*, 705–712. https://doi.org/10.1306/d4268d74-2b26-11d7-8648000102c1865d

44. Mandal, S., & Prabaharan, N. (2006). Ocean wave forecasting using recurrent neural networks. *Ocean Engineering, 33*(10), 1401–1410. https://doi.org/10.1016/j.oceaneng.2005.08.007

45. McCuen, R. H., Knight, Z., & Cutter, A. G. (2006). Evaluation of the Nash–Sutcliffe efficiency index. *Journal of Hydrologic Engineering, 11*(6), 597–602. https://doi.org/10.1061/(ASCE)1084-0699(2006)11:6(597)

46. Chai, T., & Draxler, R. R. (2014). Root mean square error (RMSE) or mean absolute error (MAE)? Arguments against avoiding RMSE in the literature. *Geoscientific Model Development, 7*(3),

1247–1250. https://doi.org/10.5194/gmd-7-1247-2014

47. Valipour, A., & Shirgahi, H. (2022). Estimation of rip density on intermediate beaches using an extreme learning machine model. *Regional Studies in Marine Science, 52*, 102332. https://doi.org/10.1016/j.rsma.2022.102332